In Situ Identification of Spherical Ag Monomers and Dimers at Zeptomole Adsorbate Concentrations by Surface-Enhanced Raman Scattering Correlation Spectroscopy

Aude Barbara, Fabien Dubois, Pascal Quemerais

In situ Identification of Spherical Ag Monomers and Dimers at Zeptomole Adsorbate Concentrations by SERS Correlation Spectroscopy

Aude Barbara[†],* Fabien Dubois[†], and Pascal Quémerais[†]

[†]*Institut Néel CNRS/UGA, F-38042 Grenoble Cedex 9, France*

E-mail: aude.barbara@neel.cnrs.fr

Abstract

We have developed a bright optical setup especially optimized for surface enhanced Raman scattering correlation spectroscopy. We show that the brightness of the experiment combined with the correlation approach permits *in situ* access to the size and shape of the SERS-active aggregates in solution despite a very weak SERS signal of the adsorbed molecules. As a result we demonstrate that dimers and larger SERS-active aggregates can be identified through the temporal fluctuations of the SERS signal of only a few hundred of adsorbed molecules i.e at zeptomole adsorbate concentrations. Monomers covered by a monolayer of MBA were also identified. These results open a way for single nanoparticle sensing, for single molecule SERS-active aggregate characterization or for quantitative monitoring of functionalization processes on metallic objects.

Introduction

Surface enhanced Raman scattering (SERS) is a phenomenon by which molecules at nanometer distances from a metallic surface may present Raman scattering cross sections enhanced by several orders of magnitude. It is therefore a widely used technique for ultra-sensitive chemical sensing, in particular since the ultimate stage of single molecule detection [1–3] was achieved. It is well established that the Raman enhancement factors (EFs) are mainly due to the plasmon resonances of the metal that induce high electric fields localization within nanogap regions of the substrate.Therefore SERS EFs strongly depend on the morphology of the metallic substrate. A key point in the control and the understanding of SERS experiments is thus the determination of the relationship between the optical and the structural properties of the metallic surfaces hosting the molecules.

Among the various SERS substrates, Ag and Au spherical colloids have attracted a massive attention [4] as they can easily be prepared via robust and low-cost wet chemistry procedures and present very strong EFs in the visible range when the nanoparticles (NPs) flocculate and form aggregates. However, these nanosize objects are difficult to image optically as they are far below the diffraction limit. Establishing a direct correlation between their sizes and shapes on the one hand and their SERS EFs on the other hand, is therefore a challenging task. This can however be done by imaging isolated NPs, dried from a colloidal solution or directly grown on a substrate, with an atomic force microscope [5] or a transmission electron microscope [6] combined with a Raman spectrometer, or by super-resolution optical imaging. [7] However most of the studies image a sample of the colloidal solutions by electron microscopy but realize the optical measurements on another sample of the solutions. The relationship between the two experiments is then assumed and this may lead to some possible misinterpretations. [8]

In a previous paper, [9] we have shown that SERS correlation spectroscopy (SERS-CS) is a very well adapted technique to overcome the issue of characterizing specifically SERS-active aggregates in colloidal solutions while measuring their SERS activity. This method, initially

proposed by Eggeling et al.[10] relies on the measurement of the SERS signal of the molecules adsorbed on metallic NPs as they diffuse through a confocal microscope.[11] This creates temporal fluctuations of the measured SERS signal and their statistical analysis leads to the determination of hydrodynamic translational and rotational diffusion times of the NPs, which are both related to their sizes. However, in this original paper as well as in more recent ones,[12,13] SERS-CS was not exploited for its particle sizing potential and only the rotational time was analyzed to perform statistical characterizations of the SERS activity of NP aggregates. In parallel, the analysis of the translational coefficient of the particle via SERS-CS was proposed to study the surface interactions[14] or via SERS measurements combined with NP tracking to determine the size distribution of the SERS-active clusters in solution.[15] We were the first group[9] to show that the combined analysis of the translational and the rotational diffusion coefficients, using the appropriated hydrodynamic model, permits an unambiguous determination of the size and aggregation state of specifically SERS-active clusters. In the present paper, we extend our approach to very weak SERS signals, thereby giving a high sensibility to the method which can be exploited to characterize better metallic colloidal solutions, SERS EFs and functionalization processes which are massively used in nanoparticle technology.[16] Experiments were performed on silver colloidal solutions to which a very low concentration of 4-mercaptobenzoic acid (MBA) was added to prevent a massive aggregation of the NPs and to test the sensitivity of the experiment in such weak SERS EF conditions. Two different concentrations were studied, the first one chosen in such a way that a single self-assembled monolayer (SAM) of MBA is adsorbed on the Ag spherical monomers and a second one, fifty times lower, corresponding to only a few hundreds of molecules per NP. The experimental data show that the diffusion of a SAM MBA-covered Ag monomers can be identified. We emphasize that other techniques cannot reach such a sensitivity.[5,8] At the lower MBA concentration, the signal of the monomers was not detectable anymore while that of the dimers and larger aggregates was still accessed. In particular, the identification of aggregates formed by less than 30 NPs that present SERS enhancements two orders of

magnitude larger than the monomers, i.e not linearly dependent on the number of NP in the cluster, is an indication that hot spots regions containing only a few molecular probes were measured. Such a sensitivity was previously obtained, as metallic aggregates were proved to produce SERS EFs which are sufficient for single molecule sensing.[1,2,17] However, such sensing was obtained without any information on the nature of the aggregate supporting such EFs. By contrast, we show here that a molecular identification at a zeptomole sensitivity can be obtained together with the size and shape recognition of the NPs hosting the molecules.

Results and discussion

Ag NP sol characterization

The Ag colloidal stock solution was first characterized by standard means of SEM, DLS using a commercial apparatus, extinction spectra and Raman measurements. SEM images were difficult to record due to the formation of NaOH crystals as the drop of colloids dries. Nevertheless, spherical NPs with a physical radius $r = 8.25 \pm 2$ nm (diameter d=16.5 $\pm$ 4 nm) are observed (Fig.1a). This result is supported by the DLS measurements made on the commercial apparatus that calculates the size distribution of the NPs as a function of their number (Fig.1b). From the latter, one can see that the colloidal solution is mainly composed of NPs of hydrodynamic radius $r_H = 8.5 \pm 2.5$ nm. The difference between the physical and the hydrodynamic radius is due to charge layers surrounding the NPs in solution. Moreover, the commercial apparatus also provides the size distribution plotted as a function of the scattered intensities (Fig.1c). In this case, the estimated hydrodynamic radius is larger and is worth $r_H = 11.6 \pm 3.5$ nm. This is due to the fact that the scattered intensities are proportional to the volume of the NPs, which favors the largest NPs. Besides, the extinction spectrum presented in Fig.2a shows the expected band at 400 nm characteristic of the electrostatic plasmon resonances of the individual Ag NPs a few tens of

nanometers in diameter. This band is quite narrow and the spectrum does not present any additional resonances, thereby indicating a stable colloidal solution of rather monodisperse NPs. Finally, the Raman spectrum of the solution, plotted in Fig. 2b in the region where the MBA bands will be expected, only presents a weak water Raman band (bending mode) at 1650 cm^{-1}.[18]

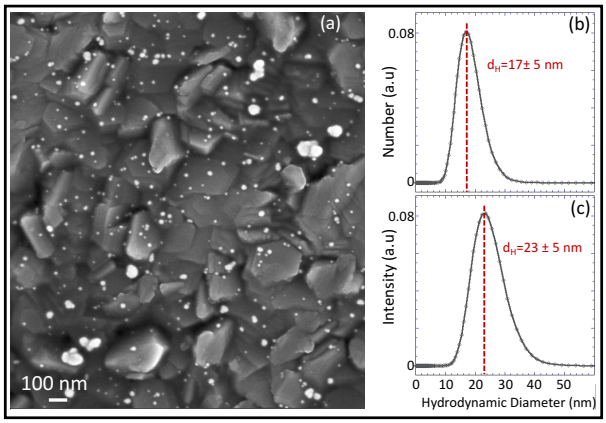

Figure 1: (a) SEM image of the Ag NPs of spherical shape. Larger NaOH crystal are also visible. (b) and (c) DLS size distributions of the NPs as a function of the number of NPs (b) and as a function of the scattered intensities (c).

A preliminary step to SERS-CS measurements was to measure the DLS ACFs of the characterized colloidal stock solution with our optical set-up. Each final ACF of the Rayleigh intensities is a sum of 2 to 5 ACFs, each one being derived from intensities acquired during 10s. The final ACF is fitted using Eq.2 to determine the different diffusion times from which the hydrodynamic radius of the NPs is obtained. $\langle N \rangle$, A_R and β are also adjusted while the values of the modulus of the scattering vector q and that of $w = 40$ are fixed and given by the experimental set-up.[19] Importantly, using our experimental set-up, DLS, and latter SERS-CS, measurements are always analyzed from the measured intensities. The values obtained for the hydrodynamic radii must therefore be compared to those obtained from the intensity size distribution of the commercial DLS apparatus. Fig.2c shows a DLS ACF fitted with $\tau_C = 40\mu$s and $\tau_D = 2.5$ ms and without considering a rotational characteristic time τ_R that should appear in the μs range. The absence of τ_R directly signs

the spherical shape of the NPs while $\tau_C = 1/q^2 D_D$ permits to access the diffusion coefficient D_D of the NPs. The hydrodynamic radius r_H of the NPs is then calculated using the Stockes-Einstein relation described for spherical moving species: $r_H = k_B T/6\pi\eta D_D$, where k_B is the Boltzmann constant and η and T are the viscosity and the temperature of the solution respectively. As the experiments were conducted at a room temperature $T = 23°$ C where $k_B T/\eta = 4.38 \times 10^{-18}$ m^3.s^{-1}, $\tau_c = 40\mu s$ corresponds to a hydrodynamic radius $r_H = 9.2$ nm. Finally, the translational diffusion time ($\tau_D = r_0^2/4D_D$) gives access to the value of r_0 that will be necessary for the SERS-CS measurements interpretation. Due to a slight size dispersion and to a small confocal volume containing only a few NPs, statistical changes of these parameters occur from one measurement to another. Fig. 2d shows a DLS ACF for which $\tau_C = 60\mu$s and $\tau_D = 3.5$ ms, which corresponds to $r_H = 13.7$ nm. This leads to an average value of $r_H = 11.5 \pm 2$ nm which is in full agreement with the intensity size distribution obtained from the commercial apparatus. The two ACFs of Figs.2c and d were also fitted with $1/\langle N \rangle = 0.9$ and $1/\langle N \rangle = 0.126$ respectively, which leads to an average concentration $C = \langle N \rangle / V_C \sim 0.9 \pm 0.7 \times 10^{12}$ NP/mL. This value is consistent with the upper-limit concentration value $C' \sim 3.6 \times 10^{12}$ NP/mL estimated from the synthesis parameters and the ratio of the total initial Ag mass to that of a spherical NP of physical radius $r = 8.25$ nm.

SERS-CS on MBA-covered NPs

Ag monomers SAM-MBA-covered identification

To conduct the SERS-CS experiments, p-MBA molecules were used as SERS probes. When MBA is added to the colloidal solutions, the molecules spontaneously adsorb on the silver NPs through Ag-S and COO^- bonds,[20,21] which leads to a more or less rapid instability of the colloids, depending on the MBA concentration and the pH of the solution.[22] In order to limit the flocculation of the NPs but still maintain a sufficiently large number of molecules, a 20 μM ethanol solution MBA was first added to the Ag colloidal solution. This concentration

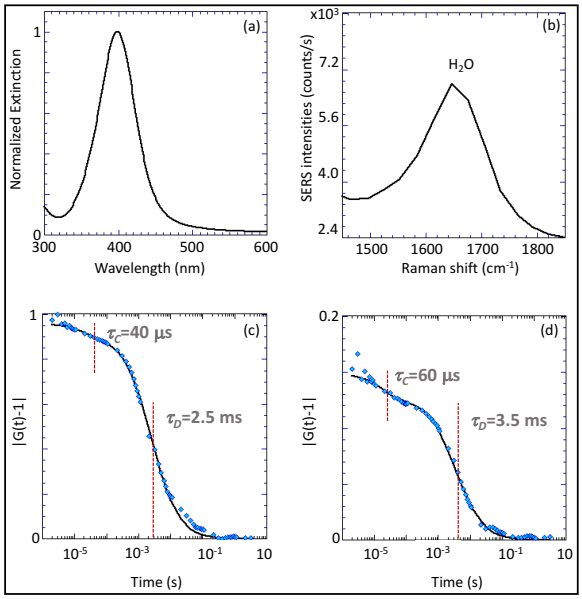

Figure 2: Characterization of the Ag colloidal solution. (a) Normalized extinction spectrum presenting the plasmon resonance band at $\lambda = 400$ nm, (b) Raman spectrum where only a weak water band is present in the region of interest and (c) and (d) DLS ACF. Measured ACFs (blue diamonds) are fitted (black line) by Eq. 2 using the characteristic times of coherence τ_C and of translational diffusion τ_D indicated in the figures. They correspond to NPs of hydrodynamic radius $r_H = 9.2$ nm (c) and $r_H = 13.7$ nm (d) depending on the nature of the NPs in the confocal volume.

is slightly larger than the 15 μM value calculated to form a self-assembled monolayer (SAM) of MBA molecules on the NPs at the estimated size and concentration, considering a MBA packing density of 5 molecules.nm^{-2}.[22] The formation of a uniform MBA SAM on the NPs was thus presumed. Extinction spectra were recorded during the first hours after MBA addition. Right upon addition, the band at 400 nm undergoes a slight red-shift of 2 nm and a widening on its long-wavelength side. After a minute, the main peak starts to diminish in intensity while its widening increases until it forms a second weak peak around 530 nm after 60 minutes (see Fig. 3a). These observations sign the slow formation of a few NP aggregates after addition of the MBA, the single monomers being still predominantly present in number after an hour.

Figure 3b presents the SERS spectra measured 2 min and 30 min after addition of the MBA. After 30 min, the MBA SERS band at 1590 cm^{-1} is clearly visible, reaching $\sim$ 20000 counts/s. SERS-CS conducted on this MBA SERS band were realized by acquiring 5 to 10 ACFs, each one being derived from intensities acquired during 10 s, which is a small time span as compared to the kinetics of the sample. The ACF obtained, displayed in Fig.3c, can be fitted by considering two characteristic times τ_D=3.5 ms and $\tau_R = 4\mu s$ and in the absence of the coherent characteristic time τ_C. This fact is expected as the Raman scattering from the different molecules is not a coherent process. As for the rotational time, its presence indicates the diffusion of an anisotropic object that can be identified by the analysis of τ_D and τ_R. The latter object being formed by the coagulation of spherical NPs, we analyse (see Ref.9 for details) the characteristic times using the so-called hydrodynamic bead model that considers the aggregates as being (flexible or rod-like) linear chains of spherical monomers.[23–25] Following these hydrodynamical theories, the translational and rotational diffusion coefficients of a chain composed of n NPs will write as $D_D^n = \alpha(n)D_D$ and $D_R^n = \beta(n)D_R$ respectively, where D_D (resp. $D_R = k_BT/8\pi\eta r_H^3$) is the translational (resp. rotational) diffusion coefficient of the monomers forming the chain, accordingly to the Stokes-Einstein theory. For dimers, $\alpha(2) = 0.72$,[24,25] so that the measured characteristic

time $\tau_D = 3.5$ ms corresponds to a dimer formed by two monomers of radius $r_H = 9.75$ nm and $\beta(2) = 0.266$,[25] so that the measured characteristic time $\tau_R = 4\mu$s corresponds to a dimer formed by two monomers of radius $r_H = 10$ nm. On the one hand, these two radius values are consistent one with the other. On the other hand, they are also consistent with the estimation of the monomers NPs size in the stock solution. It is only the combination of these both consistencies that permits to identify the measured SERS ACF as resulting from a dimer of 10 nm-radius monomers.[9]

At the shorter time after MBA addition, the MBA SERS band at 1590 cm^{-1} is quite weak ($\sim$ 1250 counts/s) and partially convoluted with the Raman band of water. SERS-CS experiments were nevertheless conducted on this MBA SERS band. The ACF obtained, displayed in Fig.3c, presents a unique characteristic time $\tau_D = 2.6$ ms. The disappearance of the rotational characteristic time signs the isotropic scattering of the MBA molecules and therefore the isotropy of their hosting NPs. Moreover, the measured τ_D corresponds to a hydrodynamic radius of 9.6 nm which is the value expected for the non-aggregated NPs in solution. Finally, if this characteristic time was to correspond to dimers whose rotational time was not detected, it would correspond to dimers formed by NPs with a hydrodynamic radius r_H=6.6 nm, according to the bead model, which is an unrealistic value. We can therefore conclude that this ACF results from the diffusion of monomers covered by MBA molecules as firstly observed in Ref. 9. Beyond this ACF analysis, the examination of the averaged SERS intensities also can give arguments in favor of the challenging identification of monomers by SERS-CS. Authors generally report on the non-observation of the SERS signal of molecules on a few monomers,[5,8] however off-resonance SERS experiments of SAM of MBA adsorbed on spherical Ag NPs were previously reported[26] on an assembly of $\sim$ 200 dried NPs and using a Raman spectrometer having a good spectral resolution. In our case, we measure only typically 5 NPs at a time, but using an incident power one order of magnitude larger and an optical set-up also one order of magnitude brighter due to the poor spectral resolution. Our experimental conditions are thus close to those described in

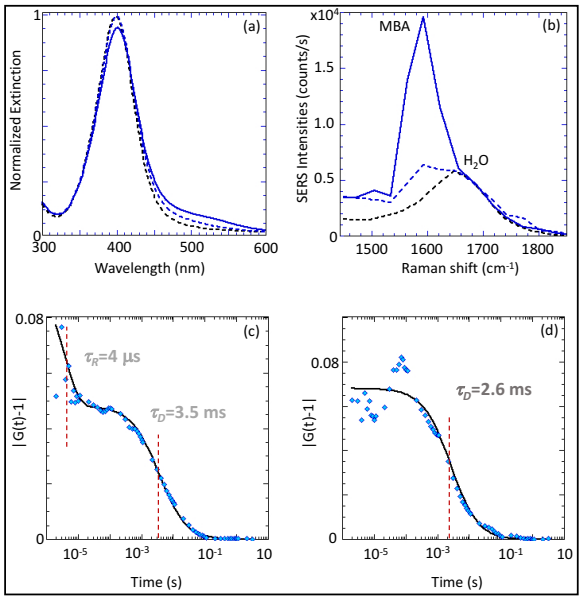

Figure 3: Characterization of the Ag colloidal solution with 20μM of MBA and identification of SAM MBA-covered monomers and dimers. (a) Extinction spectra measured after 1 min (blue dashed line) and 60 min (blue line) of MBA incubation. The extinction spectrum of the stock solution is also represented for comparison (black dashed line), (b) SERS spectra measured after 2 min (blue dashed line) and 30 min (blue line) of MBA incubation. The Raman spectrum of the stock solution is also represented for comparison (black dashed line) and (c) and (d) SERS ACFs measured after 25 min (c) and 1 min (d) of MBA incubation. Measured ACFs (blue diamonds) are fitted (black line) using Eq. 1 with the characteristic times indicated in the figures.

ref.[26] Moreover, the dynamical approach of our experiment favors the signal to noise ratio by efficiently extracting a weak signal from the background signal[27] (that does not present any correlation signature), in contrast with static measurements and thereby enhancing the sensitivity of our method. Besides, the EF of the dimers can be roughly estimated from the averaged SERS intensities. The measured SERS intensities, for monomers or for dimers can write as $I_{SERS} \propto EF \times n_V \times N_S \times \%_{HotSpot}$, where EF is the EF of the monomers (or of the dimers), n_V is the number of monomers (dimers resp.) in the confocal volume, N_S is the number of molecules adsorbed on the monomers (dimers resp.) and $\%_{HotSpot}$, is the percentage of the total area of the monomers (dimers resp.) where the EF is the highest. According to Fig.3 the SERS intensities are ~ 20 times larger when dimers are identified, as compared to that of the monomers. Moreover, in the case of the dimers, the largest EF occurs typically on 1% of the total area,[28] while the surface of the highest EF is about 25% of the total area in the case of the monomers.[5] Finally, the concentration of the dimers in the solution is estimated to be roughly 10% of that of the monomers, according to the extinction spectrum of Fig.3a. Consequently the ratio of the SERS intensity measured for the dimers to that measured for the monomers is:

$$\frac{I_{Dimers}}{I_{Monomers}} = \frac{EF_{Dimer}}{EF_{Monomer}} \times \frac{n_V \times 0.1}{n_V} \times \frac{2N_S \times 0.01}{N_S \times 0.25}$$

According to the Mie theory, the electric field at the surface of a Ag 20 nm-diameter spherical NP illuminated with a 532 nm laser is 4.5 times the incident field,[29] which gives $EF_{Monomer} = 400$. This leads to an EF for the dimers equals to $EF_{Dimer} = (20 \times 400 \times 0.25/0.1 \times 0.01 \times 2) = 10^6$, which is the expected value in off-resonance conditions.[5,28] Lastly, we can note that all the SERS-CS measurements performed more than typically 20 minutes after addition of the MBA never exhibited the signature of the monomers diffusion again, even if the extinction spectra demonstrates that they were still predominantly present in the solution. The disappearance of the ACF of the monomers when brighter aggregates are

formed is also an argument in favor of the reliability of their measurements that, if they were to be artifactual, would occur randomly. This preferential observation of SERS-active aggregates, even if their number in solution is low, also further confirms that the study of colloidal solutions as a whole may be misleading. This shows the importance of having a combined information on the state of the aggregation of the different clusters and on the SERS activities.

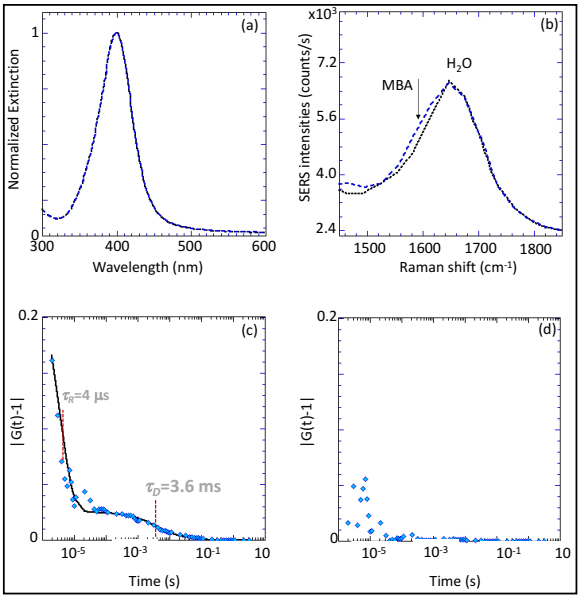

Figure 4: Characterization of the Ag colloidal solution with 0.4μM of MBA and identification of partially MBA-covered dimers. (a) Extinction spectra recorded after 60 min (blue dashed line) of MBA incubation and of the colloidal stock solution (black dashed line), (b) SERS spectrum recorded after 60 min of MBA incubation (blue dashed line) and Raman spectrum of the colloidal stock solution (black dashed line), (c) SERS ACF derived from the MBA SERS intensities 1590 cm^{-1} after 60 min of MBA incubation. Experimental data (blue diamonds) were fitted using Eq.1 (black line). The characteristic times obtained correspond to the diffusion of a dimer. (d) ACF derived from the water Raman band at 1650 cm^{-1} after 60 min of MBA incubation. Only noise is observed.

Size and shape determination of aggregates hosting zeptomole adsorbate concentration

To limit the flocculation of the NPs during a longer time and to test the sensitivity of our method further, the MBA concentration was lowered (fifty times with respect to the previous concentration). Ten μL of a 1.2×10^{-4} MBA ethanol solution was added to 3 mL of the colloidal stock solution. This leads to a final MBA concentration of 400 nM, corresponding to 2.4×10^{14} molecules per mL, that is roughly 300 to 1000 molecules per NP. Upon MBA addition the solution seems unchanged and the extinction spectrum measured after an hour of MBA incubation (Fig. 4a) is identical to that of the stock colloidal solution (without MBA). The SERS spectrum recorded after the same incubation time is shown in Fig.4b. It presents a very weak MBA SERS signal of $\sim$ 500 counts/s at 1590 cm^{-1} that appears through the broadening of the water Raman band at 1650 cm^{-1}. Despite this weak SERS signal and its strong convolution with that of the water band, SERS-CS experiments performed at 1590 cm^{-1} present low amplitudes but undeniably measurable ACFs. The AFC measured after 60 min of MBA incubation is shown in figure 4c together with the one calculated using Eq.1. A good agreement between the experimental data and the calculated ones is obtained considering here again the diffusion of a dimer of 10 nm-radius monomers. Due to the small amplitude of the ACF, considering a dimer of 12 nm-radius single NP would lead to a comparable agreement. However, in both cases, the measured ACF signs the identification of the adsorption of only a few hundreds of MBA molecules in combination with the dimeric nature of the object hosting the molecules. It is also worth noting that the possibility of an artifactual ACF was ruled out by performing SERS-CS measurements on the very near water Raman band at 1650 cm^{-1}. In this situation, the water ACF does not exhibit any clear time decay, i.e only noise is measured (Fig. 4d), and this despite Raman intensities of $\sim$ 6000 counts/s, much stronger than that of the MBA. In that case, the ACF $G(t) - 1 \approx 1/\langle N \rangle \sim 0$ as the number of water molecules in the confocal volume is very large. Here again it is the statistical analysis of the SERS intensities, via auto-correlation

functions, that permits to extract effectively the signal of the target molecules from the overall signal (here of water). This result is of great interest for trace detection approaches in cases where the signal is polluted by that of the residual molecules in the solutions or to identify functionalization processes at low adsorbate concentrations.

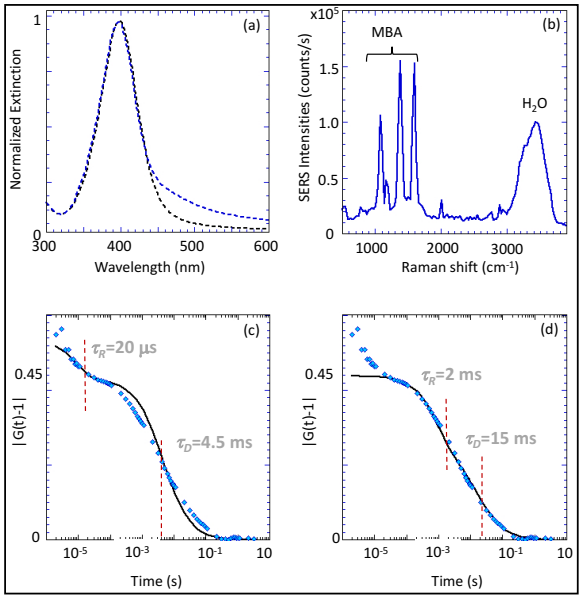

Figure 5: Characterization of the 4-weeks aged Ag colloidal solution with 0.4μM of MBA. (a) Extinction spectrum of the solution (blue dashed line) compared to that of the stock solution (black dashed line), (b) SERS spectrum and (c) and (d) SERS ACFs derived from the MBA SERS intensities at 1590 cm^{-1}. The experimental data (bue diamonds) are fitted using Eq. 1 (black line) and considering a 4-NPs chain (c) or a 25 NPs aggregate (d).

Towards single molecule SERS-active aggregates characterization

Despite the low MBA concentration, the Ag NPs in the 400 nM MBA-NPs solution slowly flocculate. After 4 weeks of aging, the solution has turned to a reddish color and the extinction spectrum, displayed in Fig. 5a, presents a wide and low amplitude broadening of the plasmonic band of the Ag monomers, signing the formation of a small amount of size-dispersed aggregates and the presence of a still significative number of non-aggregated single NPs. SERS measurements show that this small number of aggregates is responsible for a

very large SERS signal. Indeed, the MBA SERS band intensities reach $\sim 1.5 \times 10^5$ counts/s (Fig. 5b), which corresponds to an intensity ~ 300 times larger that the SERS intensities measured before the aggregation process. Figure 5c displays an ACF of the SERS intensities of the MBA band at 1590 cm^{-1}. Fitting these data is more difficult than previously as aggregates of different sizes are very likely to diffuse through the observation volume during the acquisition. Considering a unique contribution of 4-NPs chain-like aggregates ($\tau_R = 20\mu$s and τ_D=4.5 ms) allows to take correctly into account the rotational characteristic time but globally leads to a poor agreement with the experimental data (Fig. 5c). On the contrary, considering a 25-NPs aggregate for which $\tau_R = 1.9$ ms and $\tau_D = 15$ ms, (Fig. 5d) gives a better agreement but does not fit the short time decay. However, one can reasonably assume that the aggregates in solution range within these values of 4 to 25 NPs as no higher diffusion times are observed. The intensity enhancement of a factor 300 is thus not simply imputable to larger aggregates but is essentially due to the presence of molecules in hot spot regions. As already mentioned, less than 1000 molecules are adsorbed on the NPs and this represents a coverage pourcentage lower than 5%. It is consequently very unlikely that a large number of molecules stand within the hot spots. We thus believe that the SERS intensities leading to the measured ACF come from the scattering of a few tens of molecules at the most. This high sensibility of SERS-CS experiments could certainly be pushed further by creating higher SERS enhancements. This could be obtained by inducing a more controlled aggregation, by adding NaCl for instance, so that all the single NPs coagulate to form aggregates whose EM resonances stand in the laser line spectral region. Such an experiment would be close to that of Kneipp et al.[2] with a statistical approach given by the ACF instead of histograms, which would allow for a larger sampling, and thus more accurate results, and for an access to the dynamical parameters of the aggregates. In such conditions we believe that it would be possible to characterize specifically aggregates whose EFs are high enough for single molecule detection.

Conclusion

We have presented SERS-CS experiments performed on weak SERS signals to highlight the high sensitivity of our experimental setup. The weakness of the SERS signals was due to a small amount of MBA molecules adsorbed on the Ag NPs and to the off-resonance electromagnetic conditions. ACFs derived from these weak SERS intensities where analyzed through fitting procedures and using the bead hydrodynamic model. The different ACFs permitted (i) the identification of Ag monomers decorated by a MBA SAM, (ii) the identification of dimers covered by a zeptomole concentration of MBA molecules and (iii) the identification of aggregates formed by a few tens of monomers supporting EFs large enough for a few molecules sensing. These results, combined with the intrinsic advantages of the technique, namely the *in situ* and the chemically and SERS-active selective characterization, makes SERS-CS a highly promising analytical tool for targeted metal colloids and single NP sensing.

Experimental section

Colloidal solution preparation. Silver nitrate ($AgNO_3$, ACS reagent, 99%), sodium citrate tribasic dihydrate (sodium citrate, ACS reagent > 99%), ascorbic acid (reagent grade) and 4-mercaptobenzoic acid (p-MBA, 99%) were purchased from Aldrich. Sodium hydroxide (NaOH, pellets, reagent grade > 98%) was bought from Fischer Scientific. Ethanol (95%) was obtained from Sodipro. High-purity water (resistivity of 18 MΩ.cm, Millipore) was used to prepare silver nanoparticles and the samples. Filters (100 nm pores size) were purchased from Sartorius.

Citrate-coated colloidal silver nanoparticles were obtained by the reduction of silver nitrate by ascorbic acid in the presence of sodium citrate (stabilizer) in basic media, as described by Y. Qin et al.[30] The reagents were mixed together by adding 5.5 mL of a 27.3 mM water solution of sodium citrate (1.9 eq.), 5 mL of a 48 mM water solution of ascorbic acid (3 eq.) and 0.5 mL of a 1M water solution of sodium hydroxide to 80 mL of water.

After stirring for a minute at room temperature, the pH of this solution was equal to 11.2. Five mL of a 16 mM water solution of silver nitrate (1 eq.) were then rapidly added, at room temperature and under a stirring of 350 rpm. The stirring was maintained during 30 minutes after which the colloidal suspension was stocked in a glass flask. Just before being used for the experiments, the colloidal silver nanoparticles suspension was filtered through a 100 nm size filter to remove small hypothetical aggregates present after the synthesis. The optical density of the colloidal suspension measured before and after this filtration indicates that only 2.5 % of the colloidal matter was lost during this step.

Optical setup. The optical setup is schematized in Fig.6. It is composed of a confocal microscope[11] (illustrated by the objective) coupled with a monochromator used to select the wavelength of the photons to be detected by the avalanche photodiode (APD). The solutions are illuminated by a linearly polarized laser source of wavelength λ=532 nm and power P=100 mW at the sample. The incident beam is focused by a $\times$60 water immersion objective (Oympus, UPLSAPO, 1.2 NA) also used to collect the backscattered light. The confocal configuration is ensured by a 150 μm-diameter pinhole positioned at the image of the focus point which is realized by a 150 mm focal length lens tube. In such a configuration the observation volume is $V_c \sim 5\ \mu m^3$. The Rayleigh scattering is suppressed by a Notch filter of optical density of 6.0 placed in front of the pinhole while the Raman/SERS photons are transmitted and focused at the entrance a monochromator (CM110, Spectral Products)) of focal $f = 110$ mm. The entrance and output slits are 0.3 mm wide and the monochromator is equipped with a 1200 grooves/mm grating blazed at 650 nm, leading to a spectral resolution of $\sim 25\ \mathrm{cm}^{-1}$. The outgoing signal is focused on a 180 μm-diameter avalanche photodiode (APD Perkin Elmer, SPCM-AQR-15) coupled with a photon correlator (CIPRIAN) that measures the time delay between two pulses (each pulse corresponding to the arrival of a photon). This permits to record the intensity $I_\lambda(t)$ of the photons of wavelength λ as a function of time.

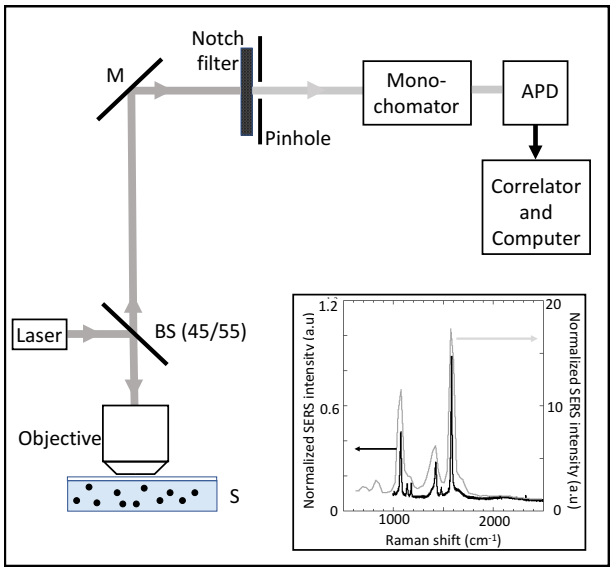

Figure 6: Optical setup for SERS/Raman spectra and SERS-CS measurements. A laser source (λ=532 nm) is focused in the sample (S) through a $\times$60 water immersion objective also used to collect the backscattered light. This backscattered light is focused onto a pinhole (P) in front of which a removable Notch filter is placed to ensure the rejection of the Rayleigh scattering. The filtered signal is then focused at the entrance of the monochromator which selects the wavelength of the outgoing photons to be detected by the avalanche photodiode (APD). Inset: SERS spectra of MBA measured with a T64000 Raman spectrometer (Horiba scientific) of focal length f = 640 mm (black) and with our optical set-up (gray). Both spectra were normalized by the Raman water band at 3400 cm^{-1}

SERS/Raman spectra SERS and Raman spectra are measured by scanning the grating of the monochromator and integrating, at each position of the grating, the intensity I(λ) over a few seconds. The relatively wide open slits, together with a small focal length, lowers the spectral resolution of the monochromator but to the benefit of a higher brightness of the set-up. A typical MBA SERS spectrum recorded by integrating the SERS intensities over 5 s per wavelength and with a wavelength step of 1 nm, is present in the inset of Fig.6. The three MBA bands, that appear at 1085 and 1590 cm^{-1} for the ν_{12} and ν_{8a} aromatic ring vibrations respectively, and at 1430 cm^{-1} for the $\nu_s(-\mathrm{COO}^-)$ vibration of the carboxylate $-\mathrm{COO}^-$ groups on the metal surface,[20] are broadened by the poor experimental spectral resolution but their intensities are twenty times larger than those measured by a conventional Raman spectrometer (here a T64000 from Horiba scientific of focal length $f = 640$ mm and 0.1 mm slit apertures) and also represented in the figure. The intensities measured with both set-ups were normalized by the Raman of the water band at 3400 cm^{-1} to enabe comparison.

SERS correlation spectroscopy SERS-CS experiments were carried out by measuring the time dependent intensity $I(t)$ of the MBA SERS band at 1590 cm^{-1}. $I(t)$ presents temporal fluctuations due to the variation of the local MBA concentration triggered by the Brownian motion of the MBA-covered NPs that brings them in and out of the focus point. These fluctuations occur with a characteristic time τ_D related to the time spent by the NP within the observation volume and with amplitudes inversely proportional to the average number of NPs present at any time in the observation volume. When the diffusing species are anisotropic, their rotation within the observation volume may also induce temporal fluctuations of the measured intensities. In our case, the latter occur due to the strong dependence of the SERS EF on the orientation of the aggregate with respect to the exciting electric field.[5] Therefore, as the aggregates turn relatively to the axial polarization of the focused beam, the SERS intensities of the molecules are modified. To access these translational and rotational diffusion coefficients, as well as the mean number of NPs in the confocal volume, a statistical analysis

of $I(t)$ is done by deriving its normalized auto-correlation function (ACF):

$$G(t) = \frac{\langle I(\tau)I(t+\tau)\rangle}{\langle I(\tau)\rangle^2}.$$

Following the theories developed for fluorescent correlation spectroscopy (FCS)[31,32] and considering a confocal volume where the light intensity profile may be described by an anisotropic Gaussian function $I(x,y,z) = I_0 e^{-2(x^2+y^2)/r_0^2 - 2z^2/z_0^2}$, I_0 being the incident laser intensity and r_0 and z_0 the radial and axial $1/e^2$ radius of the confocal volume respectively, $G(t)$ writes as:

$$G(t) = 1 + (1 + A_R e^{-t/\tau_R})\frac{c^2}{\langle N\rangle}\frac{1}{(1+t/\tau_D)(1+t/w^2\tau_D)^{0.5}}. \quad (1)$$

In this model, the NPs are considered to be independent which means that their possible collision is not taken into account. This assumption is justified by the low concentration of NPs and by the fact that if NPs collision were to happen, they would give rise to a transient SERS signal too fast to be detected. In Eq.1, τ_D and τ_R are the translational and rotational characteristic times respectively, $\langle N\rangle$ the average number of NPs in the confocal volume and A_R the parameter reflecting the degree of anisotropy of the measured NP. The other parameters do not give direct information on the NPs as $w = z_0/r_0$ is the shape parameter of the confocal volume, and $c = 1 - I/I_B$ is the background correction factor, I being the total intensity and I_B that of the background.[33] It is from the two characteristic times that the size and shape of the NPs are obtained. Indeed, the translational diffusion time of a freely diffusing NP is given by $\tau_D = r_0^2/4D_D$ where D_D is the diffusion coefficient[34] which is inversely proportional to the hydrodynamic radius of the NP while the rotational diffusion is given by the relation $\tau_D = 1/6D_R$ where D_R is the rotational coefficient[35] which is inversely proportional to the cubic power of the hydrodynamic radius of the NP. Only ACFs $G(t)$ presenting a τ_D and a τ_R corresponding to the same hydrodynamic radius can permit to determine unambiguously the size and the aggregation state of the NPs.[9] It is to be highlighted that the main advantage of SERS-CS experiments is that the moving species

are here the MBA-covered NPs since only the MBA molecules that are adsorbed on the metal can produce a measurable SERS signal and measurable fluctuations. If there were to be free MBA molecules in the solution, their (non-enhanced) Raman signal would be undetectable and even then the amplitude of the fluctuations would be too small to be measured (the Raman signal would then come from a large number $\langle N \rangle$ of molecules resulting in an AFC that tends to one, see Eq. 1). As a result, the measure of a SERS-CS ACF signs the adsorption of MBA molecules on the Ag NPs while the characteristic times of the ACF give access to the size of the NPs carrying the molecules.

Dynamic light scattering Our optical set-up can also be used for dynamic light scattering (DLS) experiments in a confocal volume.[36] In DLS, it is the elastic scattering intensity that is measured. This is achieved by removing the Notch filter and setting the grating to the Rayleigh wavelength λ =532 nm. In that case, all the NPs present in the observation volume contribute to the measured signal whether or not they are decorated by MBA molecules. A global characterization of the colloidal solution is thus accessible by DLS. Because elastic scattering is a coherent process, the measured intensities result from the interferences of the fields scattered by the NPs present in the confocal volume at the same time. These interferences depend on the relative positions of the NPs and consequently fluctuate as the NPs move. This additional source of intensity fluctuations appears as an additional term in the ACF that writes as:[36,37]

$$G(t) = 1 + \beta e^{(-t/\tau_C)} + (1 + A_R e^{-t/\tau_R}) \frac{c^2}{\langle N \rangle} \frac{1}{(1 + t/\tau_D)(1 + t/w^2\tau_D)^{0.5}}, \tag{2}$$

where $\tau_C = 1/(q^2 D_D)$ is the coherence characteristic time and q the modulus of the scattering vector with $q = 4\pi n \sin(\theta/2)/\lambda \sim 3.142 \times 10^7$ m^{-1}, n being the solution refractive index (here water, n=1.33) and θ the scattering angle (here θ=180°). β is the Siegert coefficient, a spatial coherence factor proportional to the ratio between the measured coherence area

(speckle) and the detector area.[38] Its value ranges from 0 to 1, the limiting values corresponding respectively to i) the case of a large detection area integrating many uncorrelated coherence area and ii) the case of a small detection area measuring a unique coherence area.

DLS on a commercial apparatus DLS experiments were performed on a Vasco Flex apparatus model from Cordouan Company. The samples are illuminated by a 658 nm laser source positioned at eight cm from the samples. The detection of the scattered light by an APD was recorded at 170° from the source. The ACF curves are fitted with a cumulant mathematics model that give the size distribution of the NPs, either as a function of the relative number of NPs or as a function of the scattered intensities. The latter case favors the signal of the bigger NPs, leading to higher estimation of the hydrodynamic radius of the NPs.

Extinction spectra Extinction spectra were performed using a SAFAS Xenus XC spectrophotometer. The spectra were recorded at room temperature, using a 1 cm path long quartz cuvette and 2 mm-wide slits. Baseline calibration was measured using the same cuvette filled with pure water. The solutions were diluted by a factor 6 to avoid absorption saturation. The spectra of the colloidal stock solution was normalized to one and the same normalization factor was applied to the other measurements to make the comparison between the curves easier.

Scanning Electron Microscopy Field emission scanning electron microscopy (SEM) images were recorded using a Zeiss Ultra+ scanning electron microscope. Ten mL of the nanoparticles suspension were deposited and dried on doped silicon wafers for observation.

References

(1) Nie, S.; Emory, S. R. Probing single molecules and single nanoparticles by surface-enhanced Raman scattering. *Science* **1997**, 275, 1102-1106.

(2) Kneipp, K.; Wang, Y.; Kneipp, H.; Perelman, L. T.; Itzkan, I.; Dasari, R. R.; Feld,

S. Single molecule detection using surface-enhanced Raman scattering (SERS). *Phys. Rev. Lett.* **1997**, 78, 1667-1670.

(3) Zrimsek, A. B.; Henry, A-H.; Van Duyne, R. P. Single molecule surface-enhanced Raman spectroscopy without gaps. *Phys. Chem. Lett.* **2013**, 4, 3206-3210.

(4) Surface-enhanced Raman spectroscopy, Analytical, biophysical and life science applications. Ed. S. Schlücker, Wiley-VCH Verlag 2011.

(5) Talley, C.E.; Jackson, J. B.; Oubre, C.; Grady, N. K.; Hollars, C. W.; Lane, S. M.; Huser, T. R.; Nordlander P.; Halas, N. J. Surface-enhanced Raman scattering from individual Au nanoparticles and nanoparticle dimer substrates. *Nano Lett.* **2005**, 5, 1569-1574.

(6) Camden, J. P.; Dieringer, J. A.; Wang, Y.; Masiello, D. J., Marks, L. D.; Schatz, G. C.; Van Duyne, R. P. Probing the structure of single-molecule surface enhanced Raman scattering hot spots. *J. Am. Chem. Soc.* **2008**, 130, 12616-12617.

(7) Willets, K. A.; Stranahan, S. M.; Weber, M. L. Shedding light on surface-enhanced Raman scattering hot spots through single-molecule super-resolution imaging. *J. Phys. Chem. Lett.* **2012**, 3, 1286-1294.

(8) Zhang, Y.; Walkenfort, B.; Yoon, J. H, Schlücker, S.; Xie W. Gold and silver nanoparticle monomers are non-SERS-active: a negative experimental study with silica-encapsulated Raman-reporter-coated metal colloids. *Phys.Chem.Chem.Phys.* **2015**, 17, 21120-21126.

(9) Barbara, A.; Dubois, F.; Ibanez, A.; Eng, L. M.; Quémerais, P. SERS correlation spectroscopy of silver aggregates in colloidal suspension: quantitative sizing down to a single nanoparticle. *J. Phys. hem. C* **2014**, 118,17922-17931.

(10) Eggeling, C.; Schaffer, J.; Seidel, C. A. M.; Korte, J.; Brehm, G.; Schneider, S.; Schrof, W. Homogeneity, transport, and signal properties of single Ag particles studied by single-molecule surface- enhanced resonance Raman scattering. *J. Phys. Chem. A* **2001**, 105, 3673-3679.

(11) Webb, R. H. Confocal optical microscopy. *Rep. Prog. Phys.* **1996**, 59, 427-471.

(12) Laurence, T.A.; Braun, G.; Talley, C.; Schwartzberg, A.; Moskovits, M.; Reich, N.; Huser, T. Rapid, Solution-based Characterization of Optimized SERS Nanoparticle Substrates. *J. Am. Chem. Soc.* **2009**, 131, 162-169.

(13) Laurence, T. A.; Braun, G. B.; Reich, N. O.; Moskovits, M. Robust SERS Enhancement Factor Statistics Using Rotational Correlation Spectroscopy. *Nano Lett.* **2012**, 12, 2912-2917.

(14) Asiala, S. M.; Schultz, Z. D. Surface Enhanced Raman Correlation Spectroscopy of Particles in Solution. *Anal. Chem.* **2014**, 86, 2625-2632.

(15) MacLaughlin, C. M.; Mullaithilaga, N; Yang, G.; Ip, S. Y.; Wang, C.; Walker, G. C. Surface-Enhanced Raman Scattering Dye-Labeled Au Nanoparticles for Triplexed Detection of Leukemia and Lymphoma Cells and SERS Flow Cytometry. *J. Phys. Chem. C* **2010**, 114(42), 18115-18120.

(16) Zeng, S.; Yong, K-T.; Roy, I.; Dinh, X-Q.; Yu, X.; Luan, F. A Review on Functionalized Gold Nanoparticles for Biosensing Applications, *Plasmonics* **2011**, 6, 491-506.

(17) Le Ru, E.; Meyer, M.; Etchegoin, P. G. Proof of single-molecule sensitivity in surface-enhanced Raman scattering (SERS) by means of a two-analyte technique. *J. Phys. Chem. B* **2005**, 110, 1944-1948.

(18) Brooker, M. H.; Hancock, G.; Rice, B. C.; Shapter, J. Raman frequency and intensity studies of liquid H_2O, $H_2^{18}0$ and D_20. *J. Raman Spectrosc.* **1989**, 20, 683-694.

(19) Barbara,A.; Dubois,F.; Quémerais,P.; Eng, L. M. Non-Resonant and Non-Enhanced Raman Correlation Spectroscopy. *Opt. Express* **2013**, 21, 15418-15429.

(20) Michota, A.; Bukowska, J. Surface-enhanced Raman scattering (SERS) of 4-mercaptobenzoic acid on silver and gold substrates. *J. Raman Spectrosc.* **2002**, 34, 21-25.

(21) Fleger, Y.; Mastai, Y.; Rosenbluh, M.; Dressler, D. H. Surface Enhanced Raman Spectroscopy of Aromatic Compounds on Silver Nanoclusters. *Surf. Sci.* **2009**, 603, 788-793.

(22) Yu, Y.; Handa, S.; Yajima, T.; Futamata, M. Flocculation of Ag nanoparticles elucidating adsorbed p-mercaptobenzoic acid by surface enhanced Raman scattering. *Chem. Phys. Letters* **2013**, 560, 49-54.

(23) Bloomfield, V. A. Hydrodynamic Studies of Structure of Biological Macromolecules. *Science* **1968**, 161, 1212âĹŠ1219.

(24) Adamczyk, Z.; Sadlej, K.; Wajnryb, E.; Ekiel-Jezewska, M. L.; Warszyński,P. Hydrodynamic radii and diffusion coefficients of particle aggregates derived from the bead model. *J. Colloid Interface Sci.* **2010**, 347, 192-201.

(25) García de la Torre, J.; del Rio Echenique, G.; Ortega, A. Improved calculation of rotational diffusion and intrinsic viscosity of bead models for macromolecules and nanoparticles. *J. Phys. Chem. B* **2007**, 111, 955-961.

(26) Wang, Y.; Ji, W.; Kitahama, Y.; Ruan, W.; Ozaki, Y.; Zhao, B. Exploring the Effect of Intermolecular H-Bonding: A Study on Charge-Transfer Contribution to Surface-Enhanced Raman Scattering o f p-Mercaptobenzoic Acid. *J. Chem. Phys. C* **2014**, 118, 10191-10197.

(27) Scott, B. L.; Carron, K. T. Dynamic Surface Enhanced Raman Spectroscopy (SERS): Extracting SERS from Normal Raman Scattering. *Anal. Chem.* **2012**, 84, 8448-8451.

(28) Etchegoin, P. G.; Le Ru, E. C. A perspective on Single Molecule SERS: Current Status and Future Challenges. *Phys. Chem. Chem. Phys.* **2008**, 10, 6079-6089.

(29) Bachelier G.; Private Communication and Le Ru E. C.; Etchegoin P. G. Principles of Surface-Enhanced Raman Spectroscopy and Related Plasmonic Effects, Elsevier, Amsterdam, **2009**.

(30) Qin, Y.; Ji, X.; Jing, J.; Liu, H.; Wu, H.; Yang, W. Size control over spherical silver nanoparticles by ascorbic acid reduction. *Colloids and Surfaces A : Physicochem. Eng. Aspects* **2010**, 372, 172-176.

(31) Aragón, S. R.; Pecora, R. Fluorescence correlation spectroscopy as a probe of molecular dynamics. *J. Chem. Phys.* **1976**, 64, 1791-1803.

(32) Ehrenberg, M.; Rigler, R. Rotational Brownian Motion and Fluorescence Intensity Fluctuations. *Chem. Phys.* **1974**, 4, 390-401.

(33) Thompson, N. *In* Topics in Fluorescence Spectroscopy; Lakowicz, J. R., Ed.; Plenum Press: New York, 1991; Vol. I.

(34) Einstein, A. On the motion of small particles suspended in liquids at rest required by the molecular-kinetic theory. *Annal. der Phys.* **1905**, 17, 549-560.

(35) Cummins, H. Z.; Pike, E. R. Photon Correlation Spectroscopy and Velocimetry. **1977** Plenum Press, New York.

(36) Barbara, A.; López-Ríos, T.; Dumont, S.; Gay, F; Quémerais, P. Microscope spectrometer for light scattering investigations. *Appl. Opt.* **2010**, 49, 4193-4201.

(37) Schaefer, D. W. Dynamics of Number Fluctuations: Motile Microorganisms. *Science* **1973**, 180, 1293-1295.

(38) Siegert, A. J. F. On the fluctuations in signals returned by many independently moving scatterers. *MIT Radiation Laboratory Report.* **1943**, n° 465.

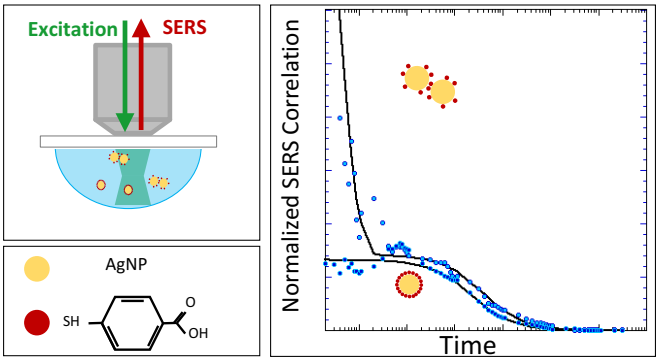
Excitation
SERS
AgNP
SH
O
OH
Normalized SERS Correlation
Time